4-5-2019

Mercury Chemostratigraphy Across the Cambrian Series 2 – Series 3 Boundary: Evidence for Increased Volcanic Activity Coincident with Extinction?

L. E. Faggetter
University of Leeds

P. B. Wignall
University of Leeds

S. B. Pruss
Smith College, spruss@smith.edu

D. S. Jones
Amherst College

S. Grasby
Geological Survey of Canada Calgary

See next page for additional authors

Follow this and additional works at: https://scholarworks.smith.edu/geo_facpubs

Part of the Geology Commons

Recommended Citation

Authors

L. E. Faggetter, P. B. Wignall, S. B. Pruss, D. S. Jones, S. Grasby, M. Widdowson, and R. J. Newton

1 **Mercury chemostratigraphy across the Cambrian Series 2 – Series 3 boundary:**

2 **evidence for increased volcanic activity coincident with extinction?**

3 Faggetter, L.E., Wignall, P.B., Pruss, S.B., Jones, D.S., Grasby, S., Widdowson, M.

4 Newton, R.J.

5

6 **ABSTRACT**

7 Flood basalt volcanism represented by the Kalkarindji Province (Australia) is

8 temporally associated with a trilobite mass extinction at the Cambrian Series 2 –

9 Series 3 boundary, providing one of the oldest potential links between volcanism and

10 biotic crisis in the Phanerozoic. However, the relative timing of flood basalt volcanism

11 (Kalkarindji Province, Australia) and the trilobite extinctions, first recorded in North

12 America, is not known. Mercury (Hg) enrichment in the sedimentary record provides

13 a potential proxy for volcanism which may facilitate improved chronologies of

14 eruption and extinction. Here we report mercury records for three sections from mid-

15 shelf strata of the Great Basin (western USA) that straddle the Series 2 – Series 3

16 boundary. One section (Oak Springs Summit, NV) features a Hg enrichment at the

17 start of the extinction interval, but mercury anomalies are also present at lower

18 levels. These older anomalies may record either earlier phases of Kalkarindji

19 volcanism, eruptions in other locations, or may be the result of sedimentary and/or

20 diagenetic processes affecting the Hg record. In the Carrara Formation at Emigrant

21 Pass, CA, the precise extinction horizon is not well defined, but a carbon isotope

22 anomaly (the Redlichiid-Olenellid Extinction Carbon isotope Event; ROECE)

23 provides a stratigraphic tie point to the Oak Springs Summit section. At Emigrant

24 Pass, Hg enrichments precede the ROECE interval and are absent in the inferred

25 extinction zone. The Pioche Formation at Ruin Wash, NV, lacks Hg enrichment at

26 the extinction horizon but contains older enrichments. The inconsistent Hg records

27 between the three sections demonstrate that factors controlling Hg accumulation and

28 preservation in marine sedimentary environments are not yet fully understood. The

29 effects of redox fluctuations may complicate one-to-one association of sedimentary

30 Hg enrichments and massive volcanism at the Cambrian Series 2 – Series 3

31 boundary and elsewhere in the geologic record.

32

33 **1. INTRODUCTION**

34   The temporal connection between large igneous province (LIP) eruptions and

35   Phanerozoic mass extinction events is well established, and the associated cause

36   and effect linkage compelling (e.g. Wignall, 2001, 2015; Courtillot and Renne, 2003;

37   Kravchinsky, 2012; Ernst & Youbi, 2017). Biotic change and carbon isotope

38   excursions are an established feature of the Cambrian, but their relationship to LIP

39   volcanism is poorly understood. In this context, the favoured candidate Cambrian LIP

40   is the Kalkarindji Province (including the Antrim lavas) of northern and western

41   Australia; this has been dated by a single zircon (Milliwindi dyke) to yield a U-Pb age

42   of 510.7 ± 0.6 Ma (Jourdan et al., 2014), demonstrating a close temporal relationship

43   to the previously reported $^{40}Ar/^{39}Ar$ date of 507.5 ± 1.6 Ma determined for its

44   extrusive portion (i.e. Antrim Lavas; Glass and Phillips, 2006). This LIP currently has

45   a surface exposure of c. 425 000 km^2 in northern and central Australia (Veevers,

46   2001), but was likely erupted over a much larger area; its scattered remnants could

47   indicate a possible original extent of >2 million km^2 (e.g. Glass and Phillips, 2006,

48   Jourdan et al., 2014). Accordingly, the province may thus be dimensionally

49   comparable with other significant Phanerozoic LIPs (e.g. Columbia River Basalts),

50   especially since it may also correlate with volcanics of similar age and/or

51   composition preserved in the Tarim Block in NW China and the North China Block (Li

52   et al., 1996; 2008), and the Sibumasu terrane preserved in current day Thailand and

53   Myanmar (Zhu et al., 2012; Cocks and Torsvik, 2013).

54   Dating of the Kalkarindji province indicates emplacement close to the

55   Cambrian Series 2 – Series 3 boundary (traditionally Lower – Middle), and thus

56   potentially contemporaneous with the extinction of the redlichiid and olenellid

57   trilobites (Palmer, 1998; Jourdan et al., 2014; Zhang et al., 2015). The extinction of

58   the olenellids has been well studied in detailed sections located in the western USA,

59   but locating the horizon that coincides with the Kalkarindji eruptions has hitherto

60   been difficult due to a lack of an eruption proxy within ancient marine sediments.

61   Temporal correlation between the Kalkarindji LIP emplacement and the Series 2 –

62   Series 3 boundary is based upon a U-Pb zircon date of 510.7 ± 0.6Ma (Jourdan et

63   al., 2014), and the provisional age of the Series 2 – Series 3 boundary (~509 Ma,

64   Ogg et al., 2016). The association of this LIP with trilobite extinction at the Series 2 –

65   Series 3 boundary is therefore inferred on the basis of this temporal correlation

66   (Glass and Phillips, 2006; Hough et al., 2006; Jourdan et al., 2014).

67   Testing a causal link between the Kalkarindji and the Series 2 – Series 3

68   trilobite extinction requires improved correlations between the volcanic event(s) and

69   the trilobite extinction horizons. Recently, mercury (Hg) concentrations in the

70   sedimentary record have provided a proxy for both regional and global volcanic

71   activity (e.g. Schuster et al., 2002, albeit in ice-core, not sediments) and thus offers

72   the potential to correlate the interval of extinction with evidence for volcanism in the

73   same stratigraphic sections. The value of this technique has been demonstrated at

74   several key mass extinction and oceanic anoxic events including those at the

75   Ordovician–Silurian; latest Permian; Permian-Triassic; end-Triassic; early Jurassic

76   and end-Cretaceous events (Sanei et al., 2012; Sial et al., 2013; 2014; Percival et

77   al., 2015; Thibodeau et al., 2016; Font et al., 2016; Grasby et al., 2013; 2016;

78   Bergquist, 2017; Gong et al., 2017; Jones et al., 2017; Percival et al., 2018). Here

79   we present sedimentary Hg records for strata in which the trilobite extinction

80   horizons have been constrained and evaluate the potential of the Kalkarindji LIP to

81   produce this sedimentary geochemical record.

82   Volcanism represents a primary source of gaseous Hg^0 to Earth's surface;

83   unlike other volcanic trace metals, its long atmospheric residence time (0.5-2 years)

84   permits hemispheric circulation and establishes its potential as a tracer for volcanism

85   (Pyle and Mather, 2003; Percival et al., 2015, 2017). Atmospheric oxidation of Hg^0

86   by halogens, ozone and radicals forms reactive Hg^{2+}, a soluble ion which is

87   deposited during precipitation (wet deposition). Horowitz et al. (2017) found that,

88   during its residence in the troposphere, Hg is most effectively oxidised by bromine

89   (Br), forming atmospheric HgBr complexes. As the largest source of atmospheric Br

90   is organobromines - which are produced as a by-product of phytoplankton

91   photosynthesis - the most effective oxidation and wet deposition of Hg^{2+} occurs

92   above and, subsequently to, the marine realm (Horowitz et al., 2017). In modern

93   oceans ~49% of marine Hg deposition occurs in tropical oceans due to the greater

94   availability of productivity-driven organobromines and other oxidising radicals at

95   these latitudes (Horowitz et al., 2017). Once in the marine realm Hg^{2+} forms

96   complexes with clay minerals (Kongchum et al., 2011), organic matter (Benoit et al.,

97   2001), and, in anoxic/euxinic conditions, it can be scavenged from seawater by

98   sulphide complexes (Benoit et al., 1999). The effective oxidation of Hg^0 by marine-

99   derived organobromines and the complexing of Hg by organics and sulphides in the

100   oceans establishes marine sediments as an efficient sink of atmospheric Hg (Benoit

101 et al., 1999; Emili et al., 2011; Horowitz et al., 2017). Therefore, marine siliciclastic

102 and carbonate rocks can act as an important repository of Hg during times of

103 heightened environmental loading (Percival et al., 2015; Grasby et al., 2016). It is

104 also worth noting that once in the atmosphere particulate Hg can also be removed

105 via "dry deposition", a portion of which may make its way into the terrestrial realm

106 (see Munthe et al., 2009 for discussion).

107   The Cambrian Period is marked by large oscillations of the inorganic carbon

108 isotope record which, at times, coincided with intensified extinction rates (Brasier et

109 al., 1994; Montañez et al., 2000; Zhu et al., 2006). At the Cambrian Series 2 – Series

110 3 boundary, a negative $\delta^{13}C$ excursion referred to as the Redlichiid – Olenellid

111 Extinction Carbon isotope Excursion (ROECE) has been documented from Laurentia

112 (Montañez, 2000; Faggetter et al., 2017), Gondwana (Schmid, 2017) and China (e.g.

113 Fan et al., 2011; Wang et al., 2011; Chang et al., 2017; Ren et al., 2017). This

114 coincides with major trilobite losses in both Gondwana and Laurentia (Montañez et

115 al., 2000; Zhu et al., 2004; 2006; Faggetter et al., 2017; Ren et al., 2017). The Series

116 2 – Series 3 boundary age (~509 Ma, Ogg et al., 2016) approximately coincides with

117 the 510.7 ± 0.6 Ma age of the Kalkarindji Province (Jourdan et al., 2014) but detailed

118 correlation is lacking. We attempt to resolve this issue by examining sedimentary Hg

119 concentrations in Cambrian Series 2 – Series 3 sections of the western USA. We

120 have analysed Hg concentrations and Hg/ total organic carbon content (TOC) from

121 two formations and three sections in the western Great Basin: Carrara Formation,

122 Emigrant Pass (Death Valley, CA) and the Pioche Formation at Oak Springs Summit

123 and Ruin Wash (Lincoln County, NV). These sections have an established

124 biostratigraphic framework, and also a record of trilobite extinction at Oak Springs

125 Summit and Ruin Wash (Webster et al., 2008; Moore and Lieberman, 2009).

126

127   **2. STUDY AREA**

128   Cambrian successions of the western Great Basin (USA) constitute the

129 primary field locations of this study. Following the breakup of the supercontinent

130 Rodinia in the late Neoproterozoic, a broad, equatorial clastic shelf developed on the

131 rapidly subsiding Laurentian margin (Prave, 1991; Howley et al., 2006). During

132 Cambrian Series 2, deposition in the Great Basin was on a broad shelf located on

133 the north-western margin of Laurentia (Fig. 1). Clastic deposition was waning and, by

134 Series 3, it had been replaced by carbonate production, resulting in the formation of

4

an extensive carbonate shelf (Fig. 1; Howley et al., 2006; Landing, 2012). We
present data from two formations spanning the Cambrian Series 2 – Series 3
boundary in the western Great Basin. The first section records the Carrara Formation
of Death Valley, exposed at Emigrant Pass, California (Fig. 2). The second section is
the Pioche Formation of eastern Nevada exposed at Oak Springs Summit (Fig. 3),
and a third section at Ruin Wash, also recording the Pioche Formation (Fig. 4). Oak
Springs Summit and Ruin Wash are close to each other (~20kms apart), whilst
Emigrant Pass is ~225km south-west of these two locations (Fig. 1). Both formations
comprise alternating siliciclastic- and limestone-dominated units (Merriam and
Palmer, 1964; Palmer and Halley, 1979; Faggetter et al., 2017). At Oak Springs
Summit and Ruin Wash, the Pioche Formation records the abrupt extinction of the
olenellid trilobites, making these two sections candidates for paired Hg-
biostratigraphic studies. At Emigrant Pass there is a paucity of trilobite fossils, but
$\delta^{13}C$ correlation, based on the record of the ROECE (e.g., Zhu et al., 2004), allows
an extinction interval to be inferred at the boundary between the Olenellus and
Eokochaspis nodosa biozones in the mid Pyramid Shale (Fig, 2; Faggetter et al.,
2017). As a further stratigraphic tie point between the two formations, the extinction
horizon within the Pioche Formation represents the top of the Olenellus biozone
(Palmer, 1998; Sundberg and McCollum, 2000).

3. METHODS

We analysed total Hg content in whole-rock powders from 93 samples taken
from the three Series 2 – Series 3 boundary sections in the western US (Figs. 2, 3,
4). The samples from Emigrant Pass and Oak Springs Summit were run at the
Geological Survey of Canada with a LECO® AMA254 mercury analyser (10%
precision, 5% relative standard deviation (RSD), Hall and Pelchat, 1997). Whole rock
powders from Ruin Wash, as well as a duplicate sample set from Oak Springs
Summit, were analysed at Amherst College (Massachusetts, USA) using a Teledyne
Leeman Labs Hydra II$_C$ mercury analyser (RSD <10%). Duplicate samples returned
a correlation coefficient of 0.99, indicating a robust positive correlation between the
results from the two laboratories.

Whole-rock powders were decarbonated using hydrochloric acid, and their
carbonate content was calculated by mass loss following acid digestion. With the
exception of Ruin Wash samples, TOC was measured from insoluble residues at the

169 University of Leeds using a LECO® SC-144DR Dual Range carbon and sulphur

170 analyser. The carbon content of insoluble residues from Ruin Wash was measured

171 with a Costech ECS 4010 elemental analyser at Amherst College in order to

172 generate TOC measurements, with RSD <5%.

173   Inorganic carbon isotope values from the Carrara Formation at Emigrant Pass

174 and Pioche Formation, Oak Springs Summit are reproduced from Faggetter et al.

175 (2017), and new inorganic carbon isotope values from Ruin Wash are presented

176 here. Whole-rock powders were analysed at the GeoZentrum Nordbayern, FAU

177 Erlangen-Nuremberg, Germany, where carbon dioxide was prepared via reaction

178 with phosphoric acid at 70°C using a Gasbench II preparation system; carbon

179 isotope ratios were measured by a ThermoFisher Delta V plus mass spectrometer in

180 continuous flow mode. Isotope ratios are reported relative to the V-PDB standard,

181 with a reproducibility of ±0.06‰ for $\delta^{13}C$ and 0.05‰ for $\delta^{18}O$.

182   Inferred redox conditions (Figs. 2, 3, 4) are based upon pyrite framboid size

183 distribution as reported in Faggetter et al. (2017); samples were assessed using a

184 scanning electron microscope (FEI Quanta 650 FEG-ESEM) in backscatter mode

185 following Bond and Wignall (2010).

186

187 ## 4. RESULTS

188 ### 4.1. TOC concentrations

189   Throughout all three sections TOC content is generally very low and exhibits

190 correlation with facies (Fig. 5). The lowest TOC values (<0.15 wt% TOC) of all three

191 sections are found in marl facies that coincide with extremely low/carbonate free

192 intervals such as the C-Shale Member of the Pioche Formation (Fig. 5). In the

193 Pioche Formation, higher TOC values are preserved in limestone of the Combined

194 Metals Member, at Oak Springs Summit where levels reach 0.48 – 2.69 wt% within

195 an oncoidal limestone of the Combined Metals Member (Fig. 5). The majority of the

196 Carrara Formation is composed of marl with very low (<0.15 wt%) TOC content, the

197 exception being horizons within the Echo Shale and Gold Ace members where

198 values span the greatest range of all three sections (<0.15 – 5.17 wt% TOC) (Fig. 5).

199

200 ### 4.2. The ROECE and trilobite extinction

201   The inorganic carbon isotope record from the Carrara Formation at Emigrant

202 Pass and the Pioche Formation at Oak Springs Summit are discussed in Faggetter

203 et al. (2017) in which a C isotope excursion of ~-3.8 ‰ is interpreted to be the

204 ROECE. Within the Pioche Formation at Oak Springs Summit, the most negative

205 inorganic carbon isotope values coincide with the extinction horizon of the olenellid

206 trilobites. ROECE is also expected to occur at Ruin Wash (Palmer 1998; Faggetter

207 et al., 2017), but the extremely low carbonate content (below detection limits) in the

208 shale of the C-Shale Member at this location does not allow measurement of a

209 continuous inorganic carbon isotope curve. The ROECE is also observed within the

210 Pyramid Shale Member of the Carrara Formation, but unlike the Pioche Formation,

211 there is no trilobite fauna to delineate a clear extinction horizon at Emigrant Pass

212 (Fig. 2). An inferred extinction interval is therefore proposed at Emigrant Pass within

213 the Pyramid Shale Member (Fig. 2), based on the biostratigraphic boundary between

214 the Olenellus Zone and the Eokochaspis nodosa Zone (Fig. 2; see Palmer and

215 Halley, 1979; Faggetter et al, 2017).

216

217   **4.3. Hg concentrations, Hg/TOC ratios and extinction**

218   The Carrara and Pioche formations contain enrichments in Hg concentrations

219 (ppb) and excursions in Hg/TOC (ppb/wt% TOC) ratios (Figs. 2, 3, 4). Hg/TOC ratios

220 from samples with extremely low TOC of <0.01 wt% C are not considered robust

221 enough to record a primary Hg signal and are not plotted in figures but are included

222 in Table 1.

223

224   4.3.1. Carrara Formation, Emigrant Pass

225   The Carrara Formation at Emigrant Pass exhibits background Hg

226 concentrations of <50 ppb throughout the section (Fig. 2). High Hg and Hg/TOC

227 values are seen in samples with both high and low TOC wt% values (Fig. 6). A

228 number of prominent enrichments occur in the lowest 90 m, with the most enriched

229 sample containing 270 ppb Hg found in the basal Eagle Mountain Shale Member.

230 Smaller enrichments recorded by one or two data points each occur in the Echo

231 Shale, Gold Ace and Pyramid Shale members. Within the ROECE interval Hg values

232 are elevated at the beginning of the $\delta^{13}C$ excursion before concentrations return to

233 low levels for the remainder of the section.

234   The Hg/TOC enrichments in the Carrara Formation occur in two distinct

235 pulses where Hg and Hg/TOC peaks correlate; an initial, multi-peak enrichment in

236 the basal 30m of the Eagle Mountain Shale Member and another during early

237 ROECE at the base of the Pyramid Shale Member (Fig. 2). It is noteworthy that

238 across the inferred extinction horizon, there are no abrupt Hg or Hg/TOC peaks and

239 values remain stable in this interval.

240

241   4.3.2. Pioche Formation, Oak Springs Summit

242   Background Hg concentrations in the Pioche Formation at Oak Springs

243 Summit are <10 ppb (Fig. 3). Highest Hg values coincide with samples with low (<0.1

244 wt%) TOC (Figs. 5 and 6). A single elevated value (46 ppb Hg) occurs in the

245 Combined Metals Member, just below the base of the ROECE, and a smaller

246 enrichment (32 ppb Hg) coincides with the most negative ROECE value and the

247 olenellid extinction horizon at the base of the C-Shale Member. Finally, there is a

248 small increase in Hg concentration (17 ppb) at ~35m in the section, which, like the

249 other enrichments, correspond to three prominent Hg/TOC spikes at Oak Springs

250 Summit (Fig. 3).

251

252

253   4.3.3. Pioche Formation, Ruin Wash

254   High Hg and Hg/TOC values are recorded in samples with both high and low

255 TOC wt% values (Fig. 6) at Ruin Wash. The Hg values are highest (up to 500 ppb) at

256 the base of the measured section in the basal ~5m of the Combined Metals Member

257 (Fig. 4). Peaks are around an order of magnitude higher than the maximum values

258 seen at Oak Springs Summit. Above the level of elevated values at Ruin Wash, Hg

259 concentrations are consistently <5 ppb, and there is no increase at the olenellid

260 extinction horizon.

261

262 **5. DISCUSSION**

263   The three sections show an inconsistent correspondence between the

264 olenellid trilobite extinction, ROECE and sedimentary Hg enrichments (Fig. 7). We

265 review possible points for correlation between sections (e.g. ROECE interval and the

266 trilobite extinction) and discuss processes which may account for the variable Hg

267 signal.

268

269 **5.1. ROECE, Hg and Hg/TOC correlation**

To assess any correlation between the timing of Hg enrichment and ROECE, we delineate the base of the excursion based on the following two criteria. Firstly, the onset of ROECE should be present within the Pyramid Shale Member of the Carrara Formation and the upper Combined Metals Member of the Pioche Formation; this is based on an abrupt negative carbon isotope excursion within the Olenellus trilobite biozone, immediately preceding the olenellid extinction (Montañez et al., 2000). Secondly, given this stratigraphic constraint, we mark the onset of the excursion as the stratigraphic base of the negative inflexion interpreted within these members, i.e. ~60 m at Emigrant Pass and ~13 m at Oak Springs Summit. Between the Carrara and Pioche formations, our data show no clear relationship between the onset of ROECE and Hg or Hg/TOC enrichments. At Emigrant Pass an enrichment occurs around 10 m above the base of ROECE and at Oak Springs Summit an enrichment occurs ~1 m below the base of the excursion. It is clear from enrichments in the Eagle Mountain Shale Member of the Carrara Formation and in the Combined Metals Member of the Pioche Formation that the majority of Hg and Hg/TOC excursions occur before the ROECE interval.

5.2. Extinction, Hg and Hg/TOC

In the Pioche Formation at Oak Springs Summit, a small Hg (32 ppb, compared to a background of <5ppb for this section) and Hg/TOC excursion corresponds closely with the extinction horizon and the top of the Olenellus biozone (Fig. 7). However, the relationship between olenellid extinction and Hg or Hg/TOC enrichment is inconsistent among the other studied sections (Figs. 3 and 7). There is no enrichment coincident with the top of the Olenellus biozone at Emigrant Pass, nor at the extinction horizon at Ruin Wash (Fig. 7).

The high levels of Hg enrichment are generally recorded low in the study sections. In the Combined Metals Member at Ruin Wash, this is seen ~15 and ~10m below the olenellid extinction level at Ruin Wash (Fig. 4), and even lower below this level at Emigrant Pass (Fig. 2). Based on the lithostratigraphic correlation of Palmer (1998), it is unlikely that the levels of Hg enrichment can be correlated with each other (Fig. 7).

The inconsistency of the relationship between Hg, ROECE and extinction across all three sections challenges the conventional use of Hg as a tracer for global environmental Hg loading in this case. Previous Hg chemostratigraphic profiles

304   invoked to trace global LIP eruptions predict, and exhibit, synchronous Hg signals

305   across regional and global sites (e.g. Percival et al., 2017). The lack of a

306   reproducible Hg signal across our sections precludes a straightforward interpretation

307   of the Hg chemostratigraphy. Our data show that only at Emigrant Pass does the

308   base of ROECE coincide with Hg enrichment, but not the duration of the isotopic

309   excursion. There is no Hg enrichment across the extinction interval.

310   The observed heterogeneity of enrichments in Hg and Hg/TOC values could

311   be caused by several factors related to environmental and diagenetic processes. Our

312   data demonstrate that volcanic loading and binding to organic matter cannot be the

313   sole drivers of the Hg record in these strata. We therefore consider the possible roles

314   that redox variations and binding to clays (and possibly sulphides) may have played

315   in controlling Hg levels.

316

317   **5.3. Hg enrichments, redox variation and TOC**

318   Previous studies have exhibited limited correlation between redox conditions,

319   organic matter deposition and Hg drawdown (e.g. Grasby et al., 2013; Percival et al.,

320   2015). However, studies from the modern suggest the redox state of the sediment

321   and water column can play an important role in mobilising or re-mobilising Hg

322   species and enhancing or diminishing Hg exchange between the sediment and water

323   column (Mason et al., 2006; Emili et al., 2011). Mercury and methyl mercury (MeHg)

324   are scavenged in oxic conditions and sequestered in the sediments; however, the

325   upward migration of the redox boundary causes Hg and MeHg to be released into

326   the water column (Emili et al., 2011; Yin et al., 2017). Emili et al. (2011) modelled Hg

327   cycling between the sediment and water column under anoxic conditions and

328   showed a strong redox control on the mobility of Hg. They found that benthic Hg flux

329   from the sediment to water column is highest during anoxic conditions and is also

330   accentuated during sulfate reduction in euxinic conditions.

331   Assessment of redox states within the Carrara and Pioche formations found

332   intermittent and locally variable periods of dysoxia during the olenellid extinction

333   interval (Webster et al., 2008; Faggetter et al., 2017). Pyrite petrography shows

334   dominantly oxygenated conditions (i.e. no framboids, scarce pyrite crystals) at

335   Emigrant Pass (Fig. 2), variably oxygenated-dysoxic-euxinic conditions at Oak

336   Springs Summit close to the extinction horizon (Fig. 3) and, euxinic to oxygenated

337   conditions across the extinction horizon at Ruin Wash (Fig. 4) (Faggetter et al.

338   2017). These fluctuating redox conditions could have altered drawdown of Hg from
339   the water column to the sediments (Horowitz et al., 2017) during times of heightened
340   Hg loading. The euxinic pyrite framboid size data from two samples at the Ruin
341   Wash trilobite extinction level do not correspond with Hg enrichment. Thus, the
342   varying behaviour of Hg under different redox conditions could underlie the differing
343   relationship between Hg and extinction in the Pioche Formation.
344   It is important to note that previously published studies reporting Hg
345   sedimentary trends across multiple sections similarly reveal variable Hg and Hg/TOC
346   ranges between localities (e.g. Grasby et al., 2016; Jones et al., 2017). Such
347   discrepancies may be an inherent component of volcanically-derived deposition and
348   fixation in marine sediments. For instance, a variable record of Hg enrichment during
349   anoxia-related extinction is reported during the Toarcian (Early Jurassic) extinction
350   (Percival et al., 2015). This event coincides with the organic-rich shales of the Jet
351   Rock in northern England, but these sediments lack the Hg enrichment that
352   otherwise might be expected given contemporaneous eruption of the Karoo-Ferrar
353   flood basalt province. Percival et al. (2015) argue that efficient organo-Hg
354   scavenging in organic-rich euxinic settings may have caused over-printing of the
355   Hg/TOC anomaly by excess organic matter deposition. However, such a mechanism
356   is unlikely in our reported Cambrian examples because TOC values in the C-Shale
357   at Ruin Wash are low (<0.3 wt %; Fig. 5). The Carrara and Pioche formations are
358   similarly characterised by low TOC and a range of Hg concentrations and Hg/TOC
359   values; we interpret this signature as showing that even in organic-poor rocks it is
360   possible to record elevated Hg concentrations during times of heightened
361   environmental loading (Figs. 5 and 6), a conclusion drawn from other organic-lean
362   records (e.g. Font et al., 2016; Percival et al., 2017). At Oak Springs Summit Hg and
363   Hg/TOC excursions occur in samples containing low TOC (<0.15 wt% C), whilst at
364   Emigrant Pass and Ruin Wash enrichments occur across a range of wt% TOC
365   values (Fig. 6). The absence of a strong correlation between Hg and TOC (Fig. 5) at
366   all three sections therefore indicates that Hg enrichment is not a function of variable
367   TOC; we therefore posit that these anomalies are not solely a function of low TOC.
368
369   **5.4. Hg and mineralogy**
370   Hg accumulation may also be controlled in part by binding to phases other
371   than organic matter. The samples analysed here exhibit very low TOC (wt%) values

372 and commonly comprise marl facies. Because clay minerals can act as an efficient

373 Hg binding medium in the absence of a larger organic matter reservoir, the

374 sediment/rock composition at the time of Hg deposition may partially control Hg

375 concentration (Zhong and Wang, 2008; Kongchum et al., 2011). High surface area

376 reactivity for clay minerals make them effective regulators of Hg in aquatic sediments

377 and up to an order of magnitude higher Hg concentrations have been found in

378 secondary minerals such as clay versus primary minerals such as quartz and

379 feldspar (Tessier et al., 1982). Higher proportions of primary silicate minerals

380 therefore have the capability to "dilute" the amount of Hg binding during Hg loading

381 (Tessier et al., 1982), and a variation in sediment composition across our study

382 location could be a contributing factor to the observed inconsistent Hg records.

383

384 **5.5. Hg as an indicator of volcanism**

385 The pre-ROECE levels of Hg enrichment observed at Emigrant Pass and

386 Ruin Wash are enigmatic, and it is currently unclear if they record an unknown local

387 volcanic source, an early eruptive pulse of the Kalkarindji LIP, or are instead a

388 response to sedimentary/diagenetic redox variations. To resolve this uncertainty,

389 further work is required to determine how widespread these perturbations are, both

390 within Laurentia and globally.

391 Challenges to linking Hg excursions with LIP volcanism are not restricted to

392 our Cambrian successions. Percival et al. (2018) present a comprehensive

393 comparison of Hg records from the Mesozoic, focussing on the coincidence of LIP

394 emplacement and ocean anoxic events, and report variable (both in Hg and

395 Hg/TOC) concentrations across sections and lithologies and also contrasting

396 evidence of Hg enrichment during periods of LIP volcanism (e.g. an absence of a

397 broad global Hg excursion during Deccan volcanism contrasting with osmium-

398 isotope records). The apparent inconsistency between these proxies is likely due to

399 the various environments, lithologies and depositional processes.

400 Although the lack of consistent Hg records between the analysed sections

401 prevents arguing definitively for a link between Kalkarindji and the extinction event at

402 this stage, it remains likely that some of the recorded Hg excursions do record an

403 expression of these LIP eruptions for the following reasons:

404 • The Kalkarindji LIP lacks a robust body of radiometric dates, Accordingly,

405 additional dating efforts within the Kalkarindji province itself may also help

clarify its emplacement history, and whether initial volcanic pulses occurred considerably earlier than current geochronological constraints suggest. Current age dating does suggest that the onset of eruption may straddle, or possibly predates the Series 2 – Series 3 boundary (Marshall et al., 2018), thus raising the possibility that the Hg record from the Great Basin records other volcanic eruptions. If this proves to be the case, then Hg anomalies may be a useful marker for independently implicating specific volcanic events, but offers limited resolution when attempting to discriminate between multiple contemporaneous sources.

- Many LIPs, whilst erupted rapidly on a geological timescale, are iterative in their eruptive behaviour and being characterised by short periods of very intense activity (Chenet et al., 2008; Vye-Brown et al., 2013). For instance, high-resolution geochronological studies have revealed that eruptions of other large igneous provinces occur in a pulsed nature, particularly the Permo-Triassic Siberian Traps (Burgess et al., 2017), the end-Triassic Central Atlantic Magmatic Province (Davies et al., 2017) and the end-Cretaceous Deccan Traps (Schoene et al., 2015). Given the evidence for pulsed LIP emplacement throughout Earth history, it is plausible that multiple eruption episodes characterise the emplacement of the Kalkarindji LIP.

- The broad-scale architecture of the province, as evidenced by the several geochemically related sub-provinces (Glass and Phillips, 2006), may indicate more than one eruptive focus during its eruptive lifetime.

- Marshall et al. (2016) report that many Kalkarindji flows were effectively degassed: such near-complete degassing could have occurred either at the vent source (Guilbaud et al., 2007) or during propagation across the evolving lava fields. Importantly, degassing occurs either during fissure eruption and associated fire-fountaining similar to that observed from Laki eruptions. Such effusions can transport volcanogenic volatiles high into the troposphere, and possibly into the stratosphere, since fire fountains, augmented by heat released from nascent flows drive thermal uplift generating buoyant ash and gas plumes (Thordarson and Self, 1998; Glaze et al., 2017). Accordingly, volatiles may be lofted high into the atmosphere (Stothers et al., 1986; Woods, 1993), and this available for distribution certainly at local and regional

439   scales or, under favourable conditions, more globally. In this context, it is

440   important to note that the Kalkarindji LIP was erupted near the equator (Fig. 1;

441   Cocks and Torsvik, 2013; Lawver et al., 2015) where the tropopause would

442   have been at a greater altitude thus mitigating against wider distribution, but

443   that atmospheric circulation patterns an equatorial location would have

444   otherwise aided in allowing aerosol distribution to both hemispheres

445   • In addition, Marshall et al., (2016) also argue for a fundamental change in

446   eruptive style; the main succession being typified by thick, inflated pahoehoe

447   flow and the overlying Blackfella Rockhole Member (BRM), which is instead

448   characterised by huge rubble-topped flows. This change in eruptive style,

449   together the occurrence of stromatolite reefs and aeolian(?) sand horizons

450   preserved within these upper eruptive units indicates that later eruptive

451   episodes occurred into a complex paleoenvironment affected by both

452   terrestrial and shallow marine conditions.

453

454   To summarise, the degree and timing of Hg release is likely to have varied

455   significantly during construction of the Kalkarindji LIP and, together with outlined

456   factors controlling lofting and circulation of volatiles, may thus help explain the

457   iterative and/or incomplete record of Hg here reported in the mid-Cambrian marine

458   sediments.

459

460

461   **6. CONCLUSION**

462   We report sedimentary Hg and Hg/TOC enrichments from both the Carrara

463   and Pioche formations of the western Great Basin, USA. These successions are

464   constrained within a biostratigraphic and chemostratigraphic framework to record the

465   Cambrian Series 2 – Series 3 boundary, and the extinction of the Laurentian

466   olenellid trilobites is observable within the Pioche Formation. The ROECE is present

467   at two of the three studied sections (Emigrant Pass, Carrara Formation and Oak

468   Springs Summit, Pioche Formation). In the Carrara Formation, the majority of Hg

469   enrichments predate ROECE, with a single enrichment occurring just above the base

470   of the excursion. At Oak Springs Summit ROECE is preceded by Hg enrichment.

471   Within the Pioche Formation at Oak Springs Summit the extinction horizon of

472   the olenellid trilobites is marked by positive Hg and Hg/TOC excursions; however, a

473 similar excursion is not apparent at the equivalent horizon from Ruin Wash. The

474 failure to locate Hg enrichment in the euxinic Ruin Wash section suggest that the

475 redox conditions were unfavourable. Our data supports the hypothesis that Hg and

476 Hg/TOC enrichments within the Carrara and Pioche formations are not solely derived

477 from enhanced TOC preservation, but that inconsistent Hg trends may have resulted

478 from variable environmental and diagenetic processes at the different sites. Given

479 the strong control anoxia exerts on Hg flux, speciation and accumulation in modern

480 settings, the role of redox states in deep time is clearly important when assessing the

481 record of Hg in rocks.

482 The timing, volume and palaeo-position of the Kalkarindji LIP makes it a key

483 candidate as the source of environmental Hg loading and subsequent enrichments in

484 the Carrara and Pioche formations. Thus, the Kalkarindji potentially contributed to

485 the Hg concentrations at the Cambrian Series 2 – Series 3 boundary, and that the

486 occurrence of precursor levels of Hg enrichment may point to hitherto unrecognised

487 phases of volcanism during construction of the Kalkarindji LIP, or else the possibility

488 of other, as yet, unknown major volcanic episodes.

489

497

498 **REFERENCES CITED**

499 Chenet, A. L., Courtillot, V., Fluteau, F., Gérard, M., Quidelleur, X., Khadri, S. F. R.,

500 Thordarson, T. (2009). Determination of rapid Deccan eruptions across the

501 Cretaceous-Tertiary boundary using paleomagnetic secular variation: 2.

502 Constraints from analysis of eight new sections and synthesis for a 3500-m-

503 thick composite section. Journal of Geophysical Research: Solid

504 Earth, 114(B6).

505 Benoit, J.M., Gilmour, C.C., Mason, R.P., Heyes, R., (1999). Sulfide controls on

506 mercury speciation and bioavailability to methylating bacteria in sediment pore

507   waters. Environ. Sci. Technol. 33, 951–957.

508   Benoit, J.M., Mason, R.P., Gilmour, C.C., Aiken, G.R., (2001). Constants for mercury

509   binding by dissolved organic matter isolates from the Florida Everglades.

510   Geochim. Cosmochim. Acta 65, 4445–4451.

511   Bergquist, B. A. (2017). Mercury, volcanism, and mass extinctions. Proceedings of

512   the National Academy of Sciences, 114(33), 8675-8677.

513   Blackburn, T. J., Olsen, P. E., Bowring, S. A., McLean, N. M., Kent, D. V., Puffer, J.,

514   Et-Touhami, M. (2013). Zircon U-Pb geochronology links the end-Triassic

515   extinction with the Central Atlantic Magmatic Province. Science, 340(6135),

516   941-945.

517   Bond, D. P., Wignall, P. B. (2010). Pyrite framboid study of marine Permian–Triassic

518   boundary sections: a complex anoxic event and its relationship to

519   contemporaneous mass extinction. Geological Society of America

520   Bulletin, 122(7-8), 1265-1279.

521   Brasier, M. D., Corfield, R. M., Derry, L. A., Rozanov, A. Y., Zhuravlev, A. Y. (1994).

522   Multiple δ13C excursions spanning the Cambrian explosion to the Botomian

523   crisis in Siberia. Geology, 22(5), 455-458.

524   Burgess, S. D., Muirhead, J. D., Bowring, S. A. (2017). Initial pulse of Siberian Traps

525   sills as the trigger of the end-Permian mass extinction. Nature

526   communications, 8(1), 164.

527   Chang, C., Hu, W., Wang, X., Yu, H., Yang, A., Cao, J., Yao, S. (2017). Carbon

528   isotope stratigraphy of the lower to middle Cambrian on the eastern Yangtze

529   Platform, South China. Palaeogeography, Palaeoclimatology,

530   Palaeoecology, 479, 90-101.

531   Cocks, L. R. M. and Torsvik, T.M. (2013). The dynamic evolution of the Palaeozoic

532   geography of eastern Asia. Earth-Science Reviews 117: 40-79.

533   Courtillot, V. E., & Renne, P. R. (2003). On the ages of flood basalt events. Comptes

534   Rendus Geoscience, 335(1), 113-140.

535   Dal Corso, J., Marzoli, A., Tateo, F., Jenkyns, H. C., Bertrand, H., Youbi, N., Cirilli, S.

536   (2014). The dawn of CAMP volcanism and its bearing on the end-Triassic

537   carbon cycle disruption. Journal of the Geological Society, 171(2), 153-164.

538   Davies, J. H. F. L., Marzoli, A., Bertrand, H., Youbi, N., Ernesto, M., Schaltegger, U.

539   (2017). End-Triassic mass extinction started by intrusive CAMP

540   activity. Nature communications, 8, 15596.

541 Emili, A., Koron, N., Covelli, S., Faganeli, J., Acquavita, A., Predonzani, S., De Vittor,
542   C. (2011). Does anoxia affect mercury cycling at the sediment–water interface
543   in the Gulf of Trieste (northern Adriatic Sea)? Incubation experiments using
544   benthic flux chambers. Applied geochemistry, 26(2), 194-204.

545 Ernst, R.E. and Youbi, N. (2017). How large igneous provinces affect global climate,
546   sometimes cause mass extinction, and represent natural markers in the
547   geological record. Palaeogeography, Palaeoclimatology, Palaeoecology. 478,
548   30-52

549 Faggetter, L.E., Wignall, P.B., Pruss, S.B., Newton, R.J., Sun, Y.D. and Crowley, S.
550   (2017). Trilobite extinctions, facies changes and the ROECE carbon isotope
551   excursion at the Cambrian Series 2-3 boundary, Great Basin, western USA.
552   Palaeogeography, Palaeoclimatology, Palaeoecology, 478, 53-66

553 Fan, R., Deng, S., Zhang, X. (2011). Significant carbon isotope excursions in the
554   Cambrian and their implications for global correlations. Science China Earth
555   Sciences, 54(11), 1686-1695.

556 Fitzgerald, W.F., Lamborg, C.H., Hammerschmidt, C.R. (2007). Marine
557   biogeochemical cycling of mercury. Chemical Reviews. 107, 641–662

558 Font, E., Adatte, T., Sial, A. N., de Lacerda, L. D., Keller, G., Punekar, J. (2016).
559   Mercury anomaly, Deccan volcanism, and the end-Cretaceous mass
560   extinction. Geology, 44(2), 171-174.

561 Glass, L. M., Phillips, D. (2006). The Kalkarindji continental flood basalt province: A
562   new Cambrian large igneous province in Australia with possible links to faunal
563   extinctions. Geology, 34(6), 461-464.

564 Glaze, L. S., Self, S., Schmidt, A., Hunter, S. J. (2017). Assessing eruption column
565   height in ancient flood basalt eruptions. Earth and Planetary Science
566   Letters, 457, 263-270.

567 Gong, Q., Wang, X., Zhao, L., Grasby, S. E., Chen, Z. Q., Zhang, L., Li, Z. (2017).
568   Mercury spikes suggest volcanic driver of the Ordovician-Silurian mass
569   extinction. Scientific Reports, 7.

570 Grasby, S.E., Sanei, H., Beauchamp, B., Chen, Z. (2013). Mercury deposition
571   through the Permo–Triassic biotic crisis. Chemical Geology, 351, 209-216.

572 Grasby, S.E., Beauchamp, B., Bond, D.P.G., Wignall, P.B., Sanei, H. (2016).
573   Mercury anomalies associated with three extinction events (Capitanian crisis,
574   latest Permian extinction and the Smithian/Spathian extinction) in NW

575   Pangea. Geological Magazine 153, 285-297.

576   doi:10.1017/S0016756815000436

577 Hall, G. E., Pelchat, P. (1997). Evaluation of a direct solid sampling atomic

578   absorption spectrometer for the trace determination of mercury in geological

579   samples. Analyst, 122(9), 921-924.

580 Horowitz, H. M., Jacob, D. J., Zhang, Y., Dibble, T. S., Slemr, F., Amos, H. M.,

581   Sunderland, E. M. (2017). A new mechanism for atmospheric mercury redox

582   chemistry: Implications for the global mercury budget. Atmospheric Chemistry

583   and Physics, 17(10), 6353-6371.

584 Hough, M.L., Shields, G.A., Evins, L.Z., Strauss, H., Henderson, R.A., Mackenzie, S.

585   (2006). A major Sulphur isotope evnt at c. 510 Ma: a possible anoxia-

586   extinction-volcanism connection during the Early-Middle Cambrian transition?

587   Terra Nova 18, 257-263. doi: 10.1111/j.1365-3121.2006.00687.x

588 Howley, R.A., Rees, M. N., Jiang, G. (2006). Significance of Middle Cambrian mixed

589   carbonate-siliciclastic units for global correlation: southern Nevada,

590   USA. Palaeoworld, 15(3), 360-366.

591 Jones, D. S., Martini, A. M., Fike, D. A. Kaiho, K. (2017). A volcanic trigger for the

592   Late Ordovician mass extinction? Mercury data from south China and

593   Laurentia. Geology, 45(7), 631-634.

594 Jourdan, F., Hodges, K., Sell, B., Schaltegger, U., Wingate, M.T. D., Evins, L.Z.,

595   Blenkinsop, T. (2014). High-precision dating of the Kalkarindji large igneous

596   province, Australia, and synchrony with the Early–Middle Cambrian (Stage 4–

597   5) extinction. Geology, 42(6), 543-546.

598 Kongchum, M., Hudnall, W. H., Delaune, R. D. (2011). Relationship between

599   sediment clay minerals and total mercury. Journal of Environmental Science

600   and Health, Part A, 46(5), 534-539.

601 Kravchinsky, V.A. (2012). Paleozoic large igneous provinces of Northern Eurasia:

602   Correlation with mass extinction events. Glob. Planet. Change 86–87, 31–36.

603   doi:10.1016/j.gloplacha.2012.01.007

604 Landing, E. (2012). The great American carbonate bank in eastern Laurentia: Its

605   births, deaths, and linkage to paleooceanic oxygenation (Early Cambrian – Late

606   Ordovician), in J. R. Derby, R. D. Fritz, S. A. Longacre, W. A. Morgan, and C. A.

607   Sternbach, eds., The great American carbonate bank: The geology and

608   economic resources of the Cambrian – Ordovician Sauk megasequence of

609   Laurentia: AAPG Memoir 98, p. 451 – 492.

610 Lawver, L.A., Dalziel, I.W.D., Norton, I.O., Gahagan, L.M., Davis, J., (2015). The

611   PLATES 2014 Atlas of Plate Reconstructions (550 Ma to Present Day), PLATES

612   Progress Report No. 374-0215, University of Texas Technical Report No. 201,

613   220p.

614 Li, Z. X., Zhang, L., Powell, C. M. (1996). Positions of the East Asian cratons in the

615   Neoproterozoic supercontinent Rodinia. Australian Journal of Earth

616   Sciences, 43(6), 593-604.

617 Li, Z. X., Bogdanova, S. V., Collins, A. S., Davidson, A., De Waele, B., Ernst, R. E.,

618   Karlstrom, K. E. (2008). Assembly, configuration, and break-up history of

619   Rodinia: a synthesis. Precambrian Research, 160(1), 179-210.

620 Marshall, P. E., Widdowson, M., Murphy, D. T. (2016). The Giant Lavas of

621   Kalkarindji: rubbly pāhoehoe lava in an ancient continental flood basalt

622   province. Palaeogeography, Palaeoclimatology, Palaeoecology, 441, 22-37.

623 Marshall, P. E., Halton, A. M., Kelley, S. P., Widdowson, M., Sherlock, S. C. (2018).

624   New 40Ar/39Ar dating of the Antrim Plateau Volcanics, Australia: clarifying an

625   age for the eruptive phase of the Kalkarindji continental flood basalt

626   province. Journal of the Geological Society, 2018-035.

627 Mason, R. P., Fitzgerald, W. F., Hurley, J., Hanson, A. K., Donaghay, P. L., Sieburth,

628   J. M. (1993). Mercury biogeochemical cycling in a stratified estuary. Limnology

629   and Oceanography, 38(6), 1227-1241.

630 Mason, R. P., Kim, E. H., Cornwell, J., Heyes, D. (2006). An examination of the

631   factors influencing the flux of mercury, methylmercury and other constituents

632   from estuarine sediment. Marine Chemistry, 102(1-2), 96-110.

633 Merriam, C. W., Palmer, A. R. (1964). Cambrian rocks of the Pioche mining district,

634   Nevada, with a section on Pioche shale faunules (No. 469). United States

635   Geological Survey Professional Paper, 569, 59

636 Monperrus, M., Tessier, E., Amouroux, D., Leynaert, A., Huonnic, P., Donard, O. F.

637   X. (2007). Mercury methylation, demethylation and reduction rates in coastal

638   and marine surface waters of the Mediterranean Sea. Marine Chemistry, 107(1),
639   49-63.

640   Montañez, I. P., Osleger, D. A., Banner, J. L., Mack, L. E., Musgrove, M. (2000).
641   Evolution of the Sr and C isotope composition of Cambrian oceans. GSA
642   Today, 10(5), 1-7.

643   Moore, R. A., Lieberman, B. S. (2009). Preservation of early and Middle Cambrian
644   soft-bodied arthropods from the Pioche Shale, Nevada, USA. Palaeogeography,
645   Palaeoclimatology, Palaeoecology, 277(1), 57-62.

646   Munthe, J., Wängberg, I., & Shang, L. (2009). The origin and fate of mercury species
647   in the natural environment. Eur. Chlor. Sci. Doss, 14.

648   Ogg, J. G., Ogg, G., Gradstein, F. M. (2016). A Concise Geologic Time Scale: 2016.
649   Elsevier.

650   Palmer, A.R. (1998). Terminal early Cambrian extinction of the Olenellina:
651   documentation from the Pioche Formation, Nevada. Journal of Paleontology,
652   72 (04), 650-672.

653   Palmer, A. R., Halley, R. B. (1979). Physical stratigraphy and trilobite biostratigraphy
654   of the Carrara Formation (Lower and Middle Cambrian) in the southern Great
655   Basin (No. 1047). United States Geological Survey Professional Paper, 1047,
656   113p

657   Payne, J.L., Lehrmann, D.J., Wei, J., Orchard, M.J., Schrag, D.P., Knoll, A.H. (2004).
658   Large perturbations of the carbon cycle during recovery from the end-Permian
659   extinction. Science 305 (5683), 506–509.

660   Percival, L.M.E., Witt, M.L.I., Mather, T.A., Hermoso, M., Jenkyns, H.C., Hesselbo,
661   S.P., Al-Suwaidi, A.H., Storm, M.S., Xu, W., Ruhl, M. (2015). Globally
662   enhanced mercury deposition during the end-Pliensbachian extinction and
663   Toarcian OAE: A link to the Karoo-Ferrar Large Igneous Province. Earth ad
664   Planetary Science Letters 428, 267-280.

665   Percival, L. M., Ruhl, M., Hesselbo, S. P., Jenkyns, H. C., Mather, T. A., Whiteside,
666   J. H. (2017). Mercury evidence for pulsed volcanism during the end-Triassic
667   mass extinction. Proceedings of the National Academy of Sciences, 114(30),
668   7929-7934.

669   Percival, L. M., Jenkyns, H. C., Mather, T. A., Dickson, A. J., Batenburg, S. J., Ruhl,

670   M., Woelders, L. (2018). Does large igneous province volcanism always perturb

671   the mercury cycle? Comparing the records of Oceanic Anoxic Event 2 and the

672   end-Cretaceous to other Mesozoic events. American Journal of Science, 318(8),

673   799-860.

674   Prave, A.R. (1991). Depositional and sequence stratigraphic framework of the Lower

675   Cambrian Zabriskie Quartzite: implications for regional correlations and the Early

676   Cambrian paleogeography of the Death Valley region of California and Nevada.

677   Geological Society of America Bulletin, 104(5), 505-515.

678   Pyle, D.M., Mather, T.A. (2003). The importance of volcanic emissions for the global

679   atmo spheric mercury cycle: Atmospheric Environment, v. 37, p. 5115–5124,

680   doi:10.1016/j.at- mosenv.2003.07.011.

681   Ren, Y., Zhong, D., Gao, C., Liang, T., Sun, H., Wu, D., Zheng, X. (2017). High-

682   resolution carbon isotope records and correlations of the lower Cambrian

683   Longwangmiao formation (stage 4, Toyonian) in Chongqing, South

684   China. Palaeogeography, Palaeoclimatology, Palaeoecology.

685   Sanei, H., Grasby, S., Beauchamp, B. (2012). Latest Permian mercury anomalies.

686   Geology 40, 63–66. http://dx.doi.org/10.1130/G32596.1.

687   Schuster, P. F., Krabbenhoft, D. P., Naftz, D. L., Cecil, L. D., Olson, M. L., Dewild, J.

688   F., Abbott, M. L. (2002). Atmospheric mercury deposition during the last 270

689   years: a glacial ice core record of natural and anthropogenic

690   sources. Environmental Science & Technology, 36(11), 2303-2310.

691   Sial, A. N., Lacerda, L. D., Ferreira, V. P., Frei, R., Marquillas, R. A., Barbosa, J. A.,

692   Pereira, N. S. (2013). Mercury as a proxy for volcanic activity during extreme

693   environmental turnover: The Cretaceous–Paleogene

694   transition. Palaeogeography, Palaeoclimatology, Palaeoecology, 387, 153-

695   164.

696   Sial, A. N., Chen, J., Lacerda, L. D., Peralta, S., Gaucher, C., Frei, R., Pereira, N. S.

697   (2014). High-resolution Hg chemostratigraphy: A contribution to the distinction

698   of chemical fingerprints of the Deccan volcanism and Cretaceous–Paleogene

699   Boundary impact event. Palaeogeography, Palaeoclimatology,

700   Palaeoecology, 414, 98-115.

701   Schmid, S. (2017). Chemostratigraphy and palaeo-environmental characterisation of

702   the Cambrian stratigraphy in the Amadeus Basin, Australia. Chemical

703   Geology, 451, 169-182.

704   Schoene, B., Samperton, K. M., Eddy, M. P., Keller, G., Adatte, T., Bowring, S. A.,

705   Gertsch, B. (2015). U-Pb geochronology of the Deccan Traps and relation to

706   the end-Cretaceous mass extinction. Science, 347(6218), 182-184.

707   Stothers, R. B., Wolff, J. A., Self, S., Rampino, M. R. (1986). Basaltic fissure

708   eruptions, plume heights, and atmospheric aerosols. Geophysical Research

709   Letters, 13(8), 725-728.

710   Sundberg, F. A., McCollum, L. B. (2000). Ptychopariid trilobites of the lower-middle

711   Cambrian boundary interval, Pioche Shale, southeastern Nevada. Journal of

712   Paleontology, 74(4), 604-630.

713   Tessier, A. Campbell, P. G., Bisson, M. (1982). Particulate trace metal speciation in

714   stream sediments and relationships with grain size: implications for

715   geochemical exploration. Journal of Geochemical Exploration, 16(2), 77-104.

716   Thibodeau, A.M., Ritterbush, K., Yager, J.A., West, A.J., Ibarra, Y., Bottjer, D.J.,

717   Berelson, W.M., Bergquist, B.A., Corsetti, F.A. (2016). Mercury anomalies and

718   the timing of biotic recovery following the end-Triassic mass extinction. Nature

719   Communications 7:11147, doi: 19.1038/ncomms11147

720   Veevers, J.J. (2001). Atlas of billion-year old earth history of Australia and

721   neighbours in Gondwanaland. GEMOC Press, Sydney, Australia.

722   Vye-Brown, C., Self, S., & Barry, T. L. (2013). Architecture and emplacement of flood

723   basalt flow fields: case studies from the Columbia River Basalt Group, NW

724   USA. Bulletin of Volcanology, 75(3), 697.

725   Wang, X., Hu, W., Yao, S., Chen, Q., Xie, X. (2011). Carbon and strontium isotopes

726   and global correlation of Cambrian Series 2-Series 3 carbonate rocks in the

727   Keping area of the northwestern Tarim Basin, NW China. Marine and

728   Petroleum Geology, 28(5), 992-1002.

729   Webster, M., Gaines, R. R., Hughes, N. C. (2008). Microstratigraphy, trilobite

730   biostratinomy, and depositional environment of the "Lower Cambrian" Ruin

731   Wash Lagerstätte, Pioche Formation, Nevada. Palaeogeography,

732   Palaeoclimatology, Palaeoecology, 264(1), 100-122.

733   Wignall, P. B. (2001). Large igneous provinces and mass extinctions. Earth-science

734   Reviews, 53(1), 1-33.

735 Wignall, P.B. (2015). The Worst of Times: How Life on Earth Survived 80 Million
736   Years of Extinction. Princeton University Press.

737 Woods, A. W. (1993). A model of the plumes above basaltic fissure
738 eruptions. Geophysical Research Letters, 20(12), 1115-1118.

739 Yin, R., Xu, L., Lehmann, B., Lepak, R. F., Hurley, J. P., Mao, J., Hu, R. (2017).
740   Anomalous mercury enrichment in Early Cambrian black shales of South
741   China: Mercury isotopes indicate a seawater source. Chemical Geology. 467,
742   159-167.

743 Zhang, W.H., Shi, X.Y., Jiang, G.Q., Tang, D.J., Wang, X.Q. (2015). Mass-
744   occurrence of oncoids at the Cambrian Series2-Series 3 transition:
745   Implications for microbial resurgence following an Early Cambrian extinction.
746   Gondwana Research 28, 432-450.

747 Zhong, H., Wang, W. X. (2008). Effects of sediment composition on inorganic
748   mercury partitioning, speciation and bioavailability in oxic surficial
749   sediments. Environmental pollution, 151(1), 222-230.

750 Zhu, M. Y., Zhang, J. M., Li, G. X., Yang, A. H. (2004). Evolution of C isotopes in the
751   Cambrian of China: implications for Cambrian subdivision and trilobite mass
752   extinctions. Geobios, 37(2), 287-301.

753 Zhu, M. Y., Babcock, L. E., & Peng, S. C. (2006). Advances in Cambrian stratigraphy
754   and paleontology: integrating correlation techniques, paleobiology, taphonomy
755   and paleoenvironmental reconstruction. Palaeoworld, 15(3), 217-222.

756 Zhu, D. C., Zhao, Z. D., Niu, Y., Dilek, Y., Wang, Q., Ji, W. H., Mo, X. X. (2012).
757   Cambrian bimodal volcanism in the Lhasa Terrane, southern Tibet: record of
758   an early Paleozoic Andean-type magmatic arc in the Australian proto-Tethyan
759   margin. Chemical Geology, 328, 290-308.

760
761
762
763 Figure captions
764   1. Cambrian global palaeogeography at 510 million years ago showing
765   approximate palaeoposition of study sections, adapted from Lawver et al.
766   (2014). Architecture of Kalkarindji LIP taken from Marshall (2016) and aligned
767   to the palaeogeographic position of Australia at 510 Ma (green outline) as
768   depicted in Lawver et al. (2014).

2. Geochemical data from Emigrant Pass, Carrara Formation: TOC wt % C, $\delta^{13}C_{org}$ (permil), Hg (ppb) and Hg/TOC (ppb/ wt % C). The position of the Olenellus - Eokochaspsis nodosa biozone boundary is from Palmer and Halley (1979) inferred redox conditions are based on framboid size distribution data (Faggetter et al. 2017).

3. Geochemical data from Oak Springs Summit, Pioche Formation: TOC wt % C, $\delta^{13}C_{org}$ (permil), Hg (ppb) and Hg/TOC (ppb/ wt % C). The position of the Olenellus - Eokochaspsis nodosa biozone boundary is from Palmer (1998), inferred redox conditions are based on framboid size distribution data from Faggetter et al. (2017). See Fig. 2 for key.

4. Geochemical data from Ruin Wash, Pioche Formation: TOC wt % C, $\delta^{13}C_{org}$ (permil), Hg (ppb) and Hg/TOC (ppb/ wt % C). The position of the Olenellus - Eokochaspsis nodosa biozone boundary is from Palmer (1998), inferred redox conditions are based on framboid size distribution data from Faggetter et al. (2017). See Fig. 2 for key.

5. Stratigraphic columns showing TOC wt % C through the Carrara and Pioche formations. See Fig. 2 for key.

6. Cross plots of TOC wt % C vs. Hg (ppb) for the Carrara and Pioche formations.

7. Summary of Hg (ppb) and Hg/TOC (ppb/ wt % C) from the Carrara and Pioche formations. The position of the Olenellus - Eokochaspsis nodosa biozone boundary is from Palmer (1998), inferred redox conditions are based on framboid size distribution data from Faggetter et al. (2017). The yellow highlight correlates the Gold Ace Member of the Carrara Formation with the Combined Metals Member of the Pioche, after Palmer (1998). See Fig. 2 for key.

Table 1. Table containing stratigraphic and geochemical data. Rows coloured in grey indicate samples excluded due to low TOC (< 0.01 wt% TOC). Rows coloured in orange indicate the extinction horizon at Oak Springs Summit and Ruin Wash.

Inset map labels: Nevada, California, Utah, Arizona, RW, OSS, EP, N, 100 km

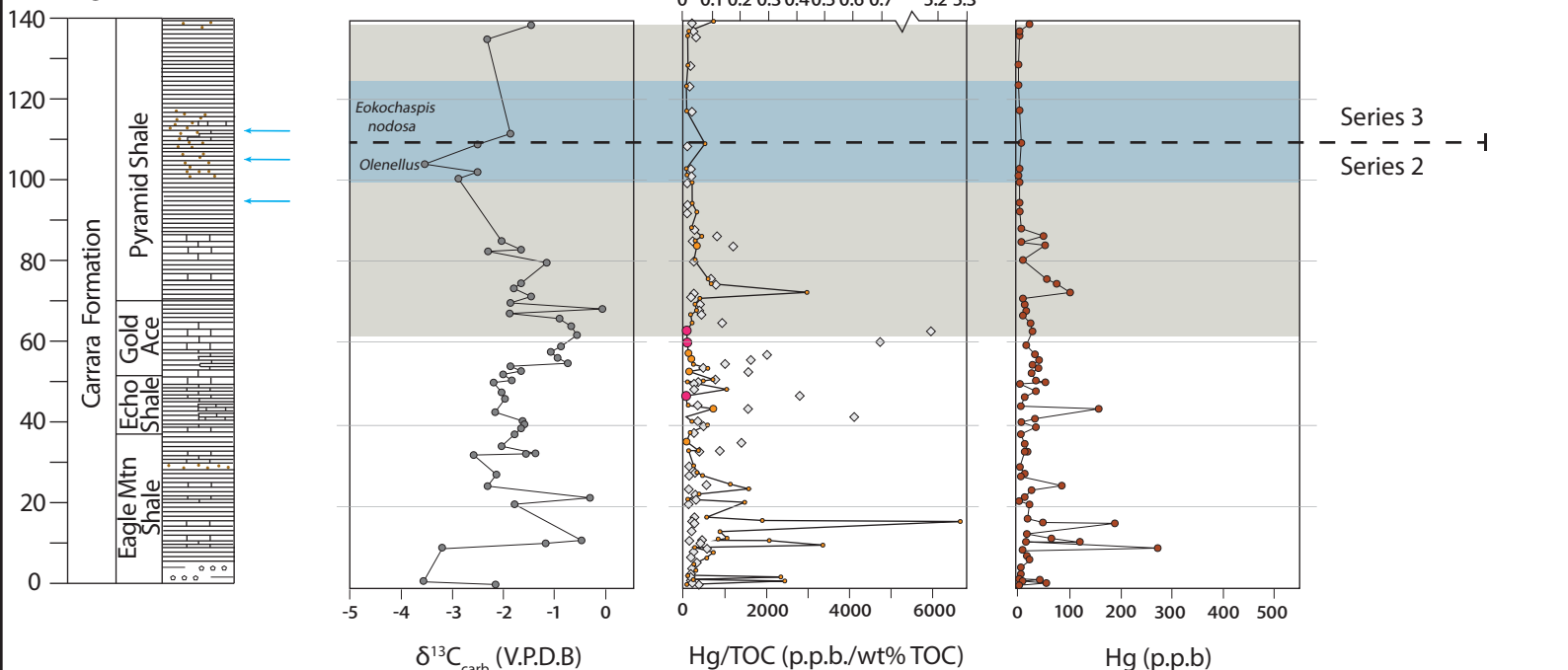510 Ma

60° N

30° N

Laurentia
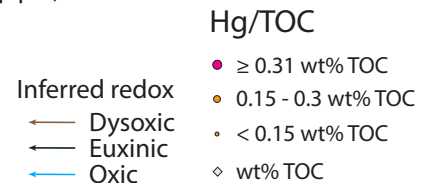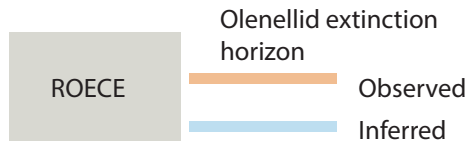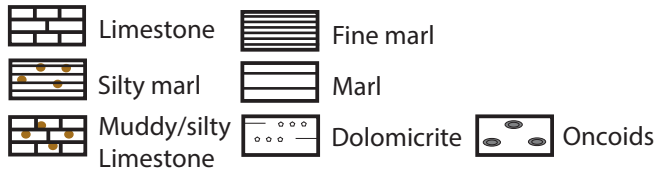
0°

Siberia

30° S

Baltica

Gondwana

Gondwana

60° S

Kalkarindji LIP
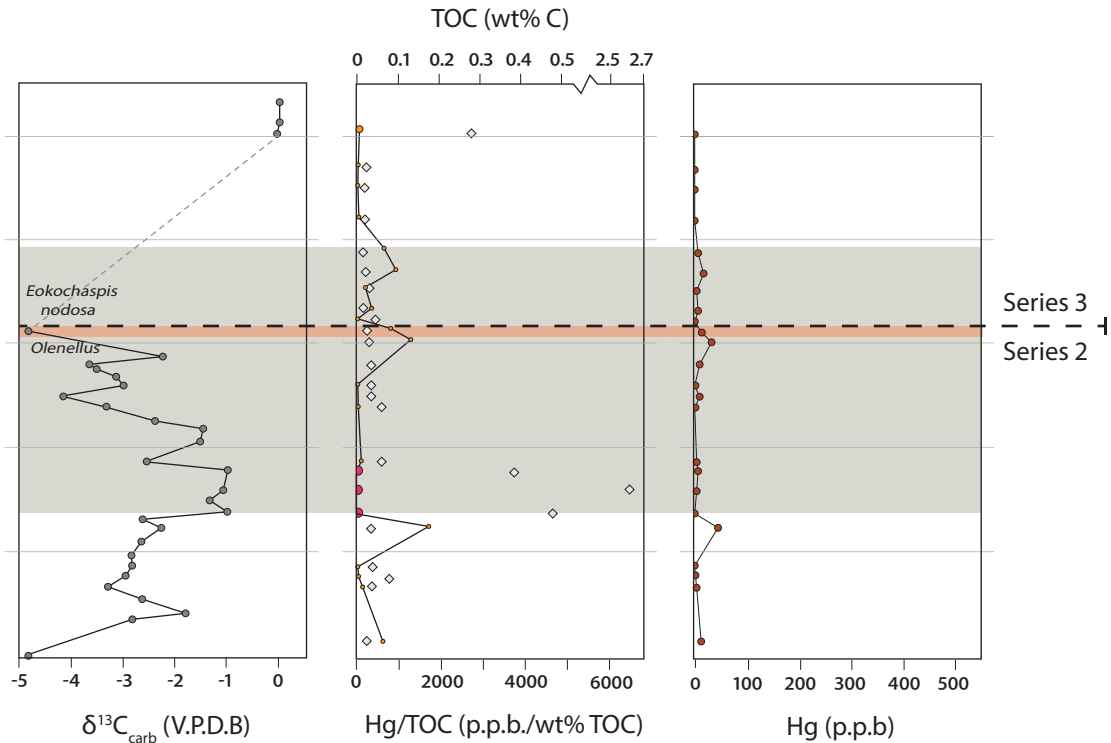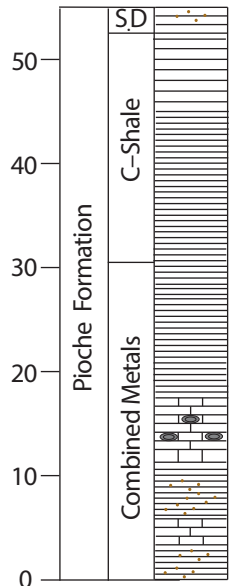
Approximate location of western Great Basin study sections

KEY

Limestone	Fine marl	
Silty marl	Marl	
Muddy/silty Limestone	Dolomicrite	Oncoids

ROECE

Olenellid extinction horizon
Observed (orange)
Inferred (blue)
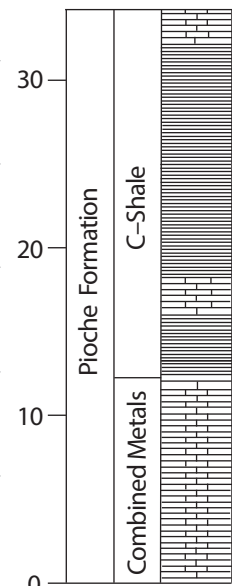
Inferred redox
Dysoxic
Euxinic
Oxic

Hg/TOC
- ≥ 0.31 wt% TOC
- 0.15 - 0.3 wt% TOC
- < 0.15 wt% TOC
- wt% TOC

Oak Springs Summit, NV.

Ruin Wash, NV.

Pioche Formation
C–Shale
Combined Metals

Eokochaspis nodosa

Olenellus

Series 3
Series 2

$\delta^{13}C_{carb}$ (V.P.D.B)

TOC (wt% C)

Hg/TOC (p.p.b./wt% TOC)

Hg (p.p.b)

Emigrant Pass, CA. — TOC (wt% C)

Carrara Formation: Pyramid Shale, Gold Ace, Echo Shale, Eagle Mtn Shale. *Eokochaspis nodosa*, *Olenellus*, S3, S2.
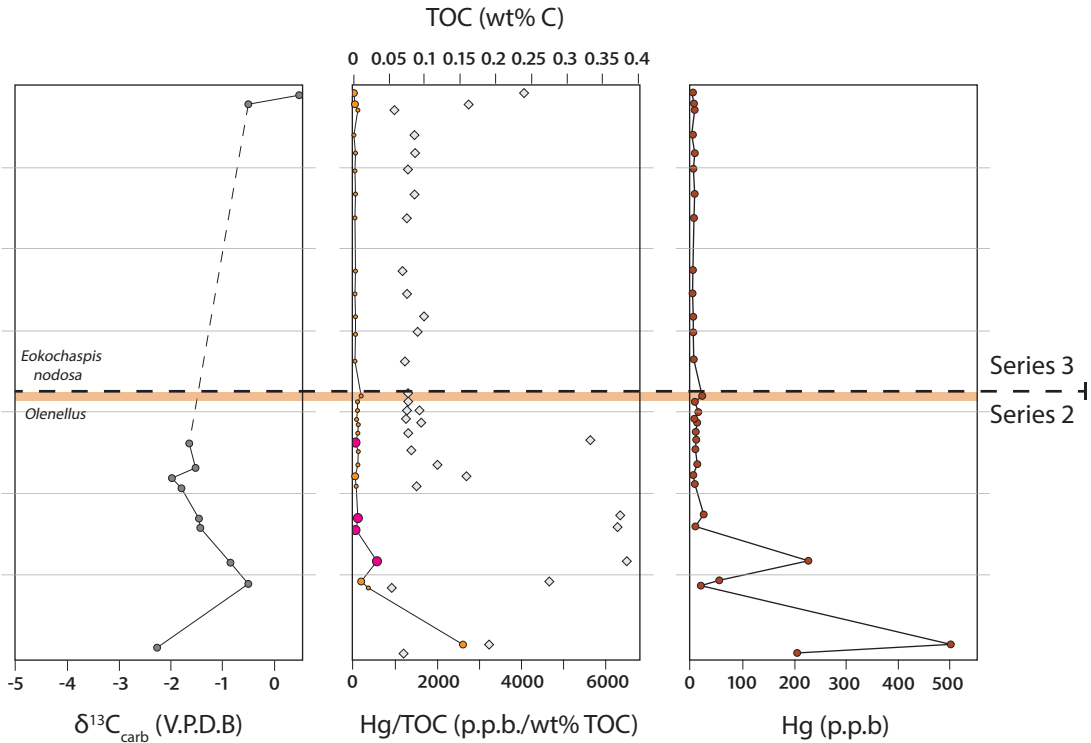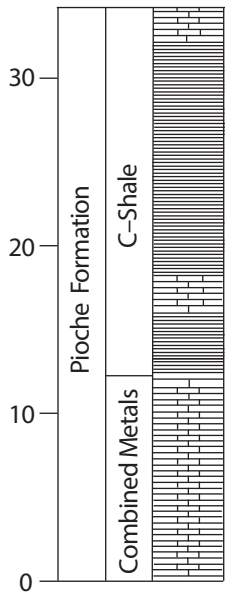
Oak Springs Summit, NV. — TOC (wt% C)

Pioche Formation: SD, C–Shale, Combined Metals. *Eokochaspis nodosa*, *Olenellus*, S3, S2.

Ruin Wash, NV. — TOC (wt% C)

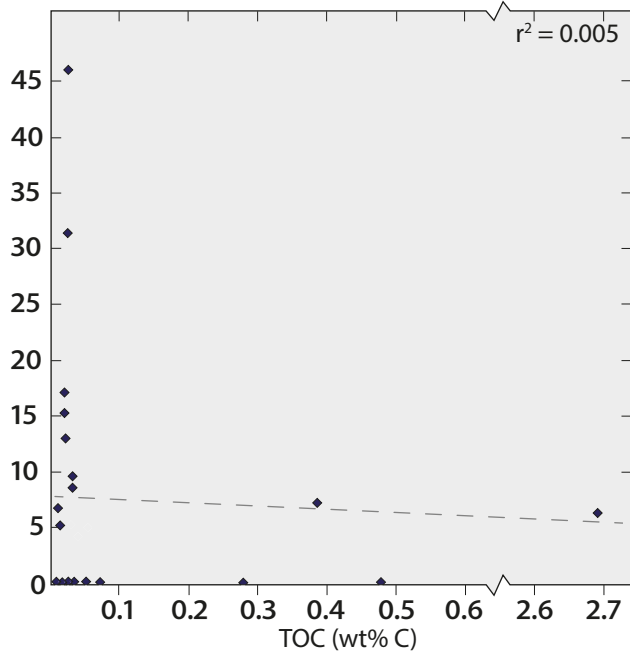Pioche Formation: C–Shale, Combined Metals. *Eokochaspis nodosa*, *Olenellus*, S3, S2.
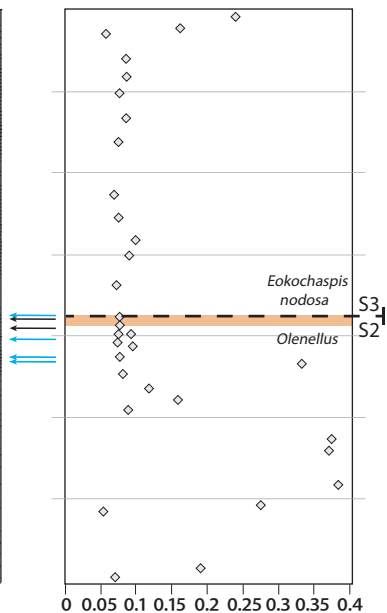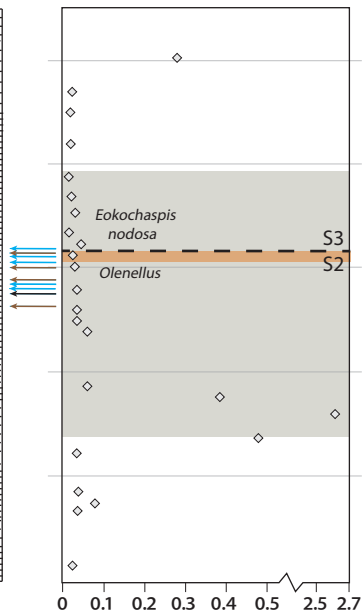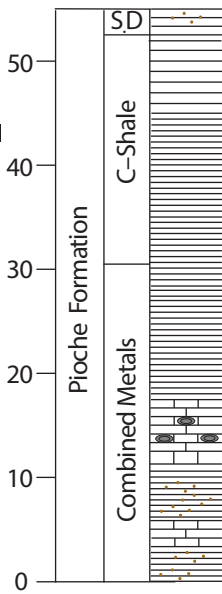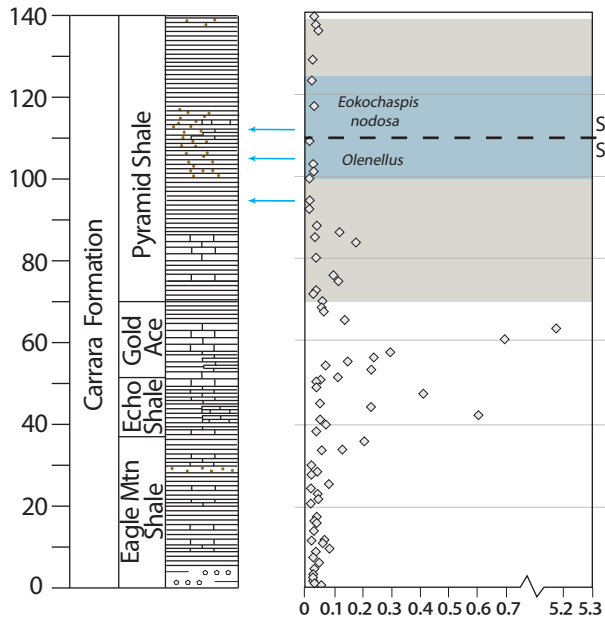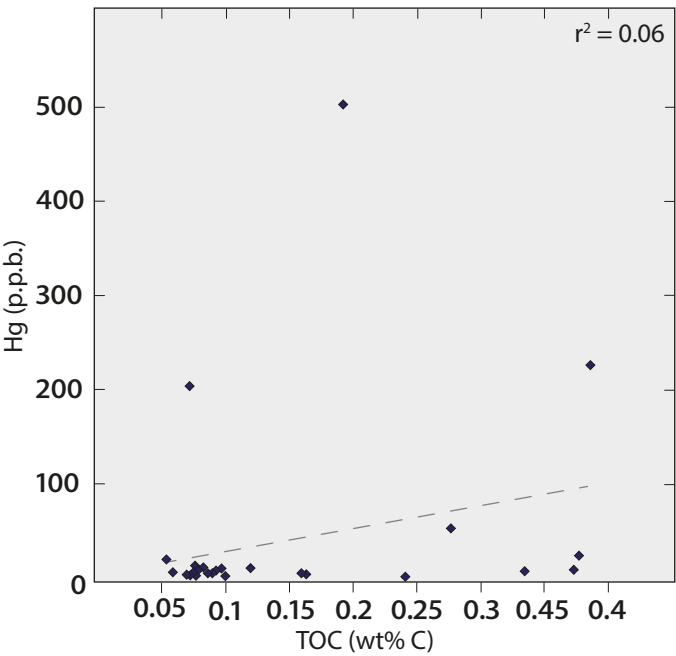
Ruin Wash, NV.   Oak Springs Summit, NV.   Emigrant Pass, CA.